Editors' Suggestion

Competing Zero-Field Chern Insulators in Superconducting Twisted Bilayer Graphene

Petr Stepanov,[1,*] Ming Xie,[2] Takashi Taniguchi,[3] Kenji Watanabe,[3] Xiaobo Lu,[1] Allan H. MacDonald,[2] B. Andrei Bernevig,[4] and Dmitri K. Efetov[1,†]

[1]*ICFO—Institut de Ciencies Fotoniques, The Barcelona Institute of Science and Technology, Castelldefels, Barcelona 08860, Spain*
[2]*Department of Physics, University of Texas at Austin, Austin, Texas 78712, USA*
[3]*National Institute of Material Sciences, 1-1 Namiki, Tsukuba 305-0044, Japan*
[4]*Department of Physics, Princeton University, Princeton, New Jersey 08544, USA*

(Received 13 April 2021; accepted 13 October 2021; published 2 November 2021)

The discovery of magic angle twisted bilayer graphene has unveiled a rich variety of superconducting, magnetic, and topologically nontrivial phases. Here, we show that the zero-field states at odd integer filling factors in *h*-BN nonaligned devices are consistent with symmetry broken Chern insulators, as is evidenced by the observation of the anomalous Hall effect near moiré cell filling factor $\nu = +1$. The corresponding Chern insulator has a Chern number $C = \pm 1$ and a relatively high Curie temperature of $T_c \approx 4.5$ K. In a perpendicular magnetic field above $B > 0.5$ T we observe a transition of the $\nu = +1$ Chern insulator from Chern number $C = \pm 1$ to $C = 3$, characterized by a quantized Hall plateau with $R_{yx} = h/3e^2$. These observations demonstrate that interaction-induced symmetry breaking leads to zero-field ground states that include almost degenerate and closely competing Chern insulators, and that states with larger Chern numbers couple most strongly to the B field. In addition, the device reveals strong superconducting phases with critical temperatures of up to $T_c \approx 3.5$ K. By providing the first demonstration of a system that allows gate-induced transitions between magnetic and superconducting phases, our observations mark a major milestone in the creation of a new generation of quantum electronics.

DOI: 10.1103/PhysRevLett.127.197701

The recently discovered quantum phases in the flat bands of $\theta_m \sim 1.1°$ magic angle twisted bilayer graphene (MATBG) include correlated insulators [1–5] (CI), superconductors [2,6–16] (SC), and correlated Chern insulators [17–25] (CCI). The CCIs can occur with different Chern numbers, and have U(4) valley-spin ferromagnetism in the bulk and topologically protected states at device edges. The search for the exact nature of these exotic phases [19,26–28] and the competition [10,29–34] between them requires a complete understanding of the role of electronic interactions in the symmetry breaking of the noninteracting fourfold spin and valley degenerate bands. The existence of multiple correlated phases in one material platform opens up new possibilities for the creation of complex gate tunable junctions [35–37].

The occurrences of CCI phases in MATBG at integer carrier filling per moiré unit cell ν is a result of electronic interactions that break the system's combined inversion and time-reversal symmetry C_2T. Breaking this symmetry can give rise to gapped valley polarized bands and to the formation of quantum Hall isospin ferromagnets [38–40] with a well-defined correspondence (C, ν) between Chern numbers C and electron fillings ν [30,31]. While theory predicts the existence of a variety of competing CCIs in zero magnetic field [29,30], some of these states have so far only been observed at elevated perpendicular magnetic field B, and hence above the critical field of the SC states. The experimental variability of the CCI state can be explained by their sensitivity to experimental parameters, such as dielectric environment [10], and complex networks of magnetic domain walls. In hexagonal boron nitride (*h*-BN) aligned MATBG devices with explicitly broken C_2 symmetry at the single particle level, CCIs with a quantized Hall conductance in zero magnetic field have been found at $\nu = +3$ [41]. However, neither SC nor CIs were observed in these devices, demonstrating that the single-particle term in the Hamiltonian that favors one sublattice over the other in aligned *h*-BN devices, alters the competition between states.

Here, we report on the first observation of anomalous Hall effect (AHE) in *h*-BN nonaligned MATBG. The AHE occurs near $\nu = +1$ filling and marks the formation of two (not yet fully quantized) $C = \pm 1$ correlated Chern insulators at $B = 0$ T. Furthermore, in elevated out-of-plane B field the device shows a sequence of perfectly quantized CCIs which follow the correspondence of (C, ν) of $(\pm 2, 0)$, $(\pm 4, 0)$, $(\pm 3, \pm 1)$, $(\pm 2, \pm 2)$, and $(\pm 1, \pm 3)$ [20–25]. We find that these high field topological CCI states can both coexist with nontopological CI states and compete with the CCI states observed in the absence of magnetic field, in particular the $(\pm 1, 1)$ and the (3, 1) states. The observation of the AHE in this particular device needs further investigation, and may be a result of twist-angle homogeneity, magnetic domain-wall size, as well as proximity to the local

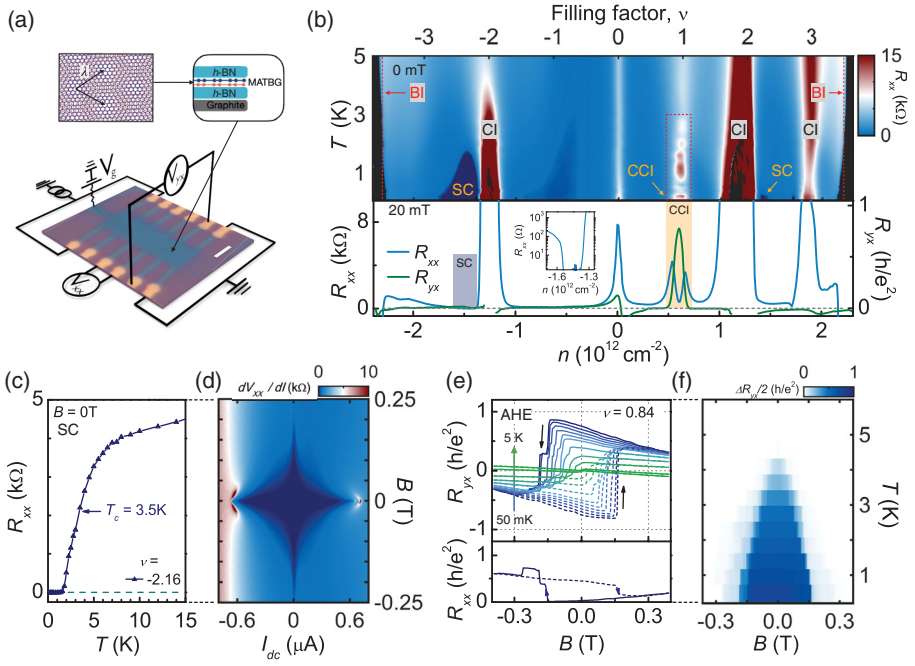

FIG. 1. (a) Optical image and transport measurement setup of the MATBG device. (b) Top: color map R_{xx} vs n and T shows the coexistence of SC, CI, and CCI states. BI denotes band insulators. Bottom: R_{xx} and R_{yx} vs n line traces at 20 mT show gate induced transitions between the SC and CCI states, with the inset showing the zero-resistance state of the SC. (c) R_{xx} vs T of the SC at optimal doping $\nu = -2.16$, shows a $T_c = 3.5$ K (50% of normal resistance). (d) dV_{xx}/dI vs I vs B in the SC state. (e) R_{yx} and R_{xx} vs B taken for increasing and decreasing B at $\nu = +0.84$. Hysteresis loops indicate an incipient Chern insulator $|C| = 1$ with (f) showing its temperature dependence with a $T_C \sim 4.5$ K.

graphite gate (∼7 nm) and heterostrain. By comparing the crystallographic edges between h-BN and graphene flakes we rule out alignment between these (extended data Fig. 1), which is supported by the fact that the resulting phase diagram [Fig. 1(b)] is in stark contrast to reported h-BN aligned phase diagrams [41,42], and shows well pronounced SC domes.

Figure 1(a) shows the optical image of the multiterminal transport device, which consists of a graphite/h-BN/MATBG/h-BN heterostructure with a twist angle of $\theta = 1.08 \pm 0.01°$ ($n_s = 2.71 \times 10^{12}$ cm^{-2}). Here, the longitudinal $R_{xx} = V_{xx}/I$ and Hall $R_{yx} = -V_{xy}/I$ resistance values are obtained from lock-in voltage measurements of V_{xx} and V_{xy}, and the source-drain current I (see Methods). The charge carrier density n is capacitively controlled with a local back gate voltage V_g on the graphite layer. We define the filling factor of carriers per moiré unit cell as $\nu = 4n/n_s$, where n_s is the density of fully filled superlattice flat band and the prefactor 4 accounts for spin and valley degeneracy of each low-energy flat band.

Figure 1(b) (top) shows the temperature and density dependent phase diagram of the device, via a color plot of R_{xx} vs n and T in zero magnetic field B, and Fig. 1(b) (bottom) shows the corresponding line traces of R_{xx} and R_{yx} vs n at base temperature $T = 30$ mK. At integer filling factors of $\nu = \pm 2$ and $\nu = +3$ we observe CIs with topologically trivial gaps $C = 0$. In addition, the device shows dome-shaped superconducting regions in the n-T phase space [Figs. 1(b) and 1(c)], which have a critical temperature of up to $T_c \approx 3.5$ K. Differential resistance dV_{xx}/dI measurements vs bias current I_{dc} and B show characteristic diamond shapes [Fig. 1(d)], and Fraunhofer oscillations (Supplemental Material Fig. 8 [43]), in very good agreement with literature [2,6,9].

In stark contrast to all previous studies of MATBG, however, at a filling of $\nu = +1$, we observe a pronounced AHE manifested by a nonzero Hall resistance at $B = 0$ T, which at $T = 50$ mK reaches a value close to the quantum of conductance $R_{yx} \approx 0.9h/e^2$ with $R_{xx} = 0$ Ω [Fig. 1(e)]. The sign of R_{yx} can be flipped by applying $B < 200$ mT, and shows a hysteresis loop between up and down sweeps. It occurs for a density range $\approx +0.6$ to $\nu \approx +1$, with a maximum at $\nu \approx +0.84$ ($n = 0.57 \times 10^{12}$ cm^{-2}) and a Curie temperature of $T_c \approx 4.5$ K [Fig. 1(f)]. These findings are notably close to previous reports on magnetism in graphene moiré heterostructures [41,42,44–46], which have been interpreted as manifestations of underdeveloped CCIs with $|C| = 1$. The absence of quantization at the present time may be due to quasiparticle delocalization, possibly assisted by transport pathways along domain walls.

We see many more CCI states at high B fields. The high B-field phase diagrams in Figs. 2(a) and 2(b) show R_{xx} and R_{yx} measurements as a function of n and B at $T = 50$ mK,

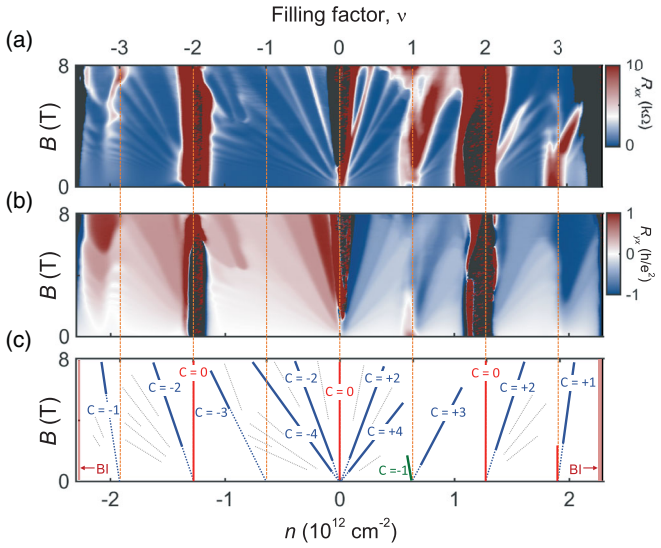

FIG. 2. (a),(b) R_{xx} and R_{yx} vs n and B. The phase space exhibits a zero-field CCI with $C = -1$ (green line) and a set of high-field CCI with $C = \pm 1$, ± 2, and ± 3 (blue lines). We observe the full set of Chern insulators emanating from partial fillings of the superlattice unit cell $(\nu, C) = (\pm 1, \pm 3)$, $(\pm 2, \pm 2)$, $(\pm 3, \pm 1)$. (c) Schematic image of (a),(b). Solid lines mark well developed CCIs, whereas dashed lines show other quantum Hall states.

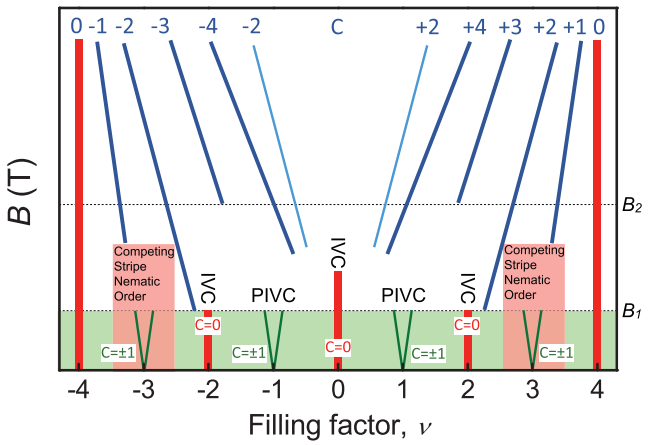

FIG. 3. Phase diagram of MATBG in a B field. Large B field favors states with the largest Chern number, which exhibit the maximum valley polarization allowed by the filling. At low B, the system undergoes phase transitions from the high-field ground states. While for $\nu = 0$ and ± 2, the many-body states are CCIs with $C = 0$ which exhibit intervalley coherence, at $\nu = \pm 3$, there is strong competition between a $C = \pm 1$ and several $C = 0$ translational or rotational symmetry broken states. Experimentally, no CCI is obtained at this filling, indicating that the CDW or nematic states win. At filling $\nu = \pm 2$, the ground state switches from $|C| = 2$ in high field to $C = 0$ at low field, in agreement with experiment. Nontrivially, at $\nu = \pm 1$, the ground state switches from $|C| = 3$ in high field to $|C| = 1$ in low field. Dark blue lines above B_1 show valley polarized CCI states. PIVC denotes partially intervalley coherent and IVC—intervalley coherent states.

and Fig. 2(c) displays the schematic of the most dominant features of the resulting Landau Fan diagram. It consists of a multitude of regions with quantized Hall conductance $R_{yx} \sim h/Ce^2$ and $R_{xx} \sim 0\ \Omega$ that follow the Streda formula [47] $dn/dB = Ce/h$, starting from different fillings ν at $B = 0$ T. In addition, we also see highly resistive CIs at fillings $\nu = \pm 2$ and $\nu = +3$ with Chern number $C = 0$. We find a clear hierarchy of gaps with indices of $(C, \nu) = (\pm 2, 0)$, $(\pm 4, 0)$, $(\pm 3, \pm 1)$, $(\pm 2, \pm 2)$, and $(\pm 1, \pm 3)$. These states are quantized at much lower fields than normal Landau level gaps and have been recently interpreted as interaction driven CCIs, which are stabilized by a small B field [20,21,23].

We compare the experimental findings with the theoretical phase diagram of MATBG [19,28–30,48] in Fig. 3, where we consider two limits: first, the flat-band limit, where the kinetic energy is artificially tuned to zero, and second, the chiral limit, where the AA-region hopping is artificially tuned to zero (the AB-region coupling is still considered). In this "chiral-flat" limit, the system enjoys a large $\mathrm{U}(4) \times \mathrm{U}(4)$ symmetry, which allows for the exact determination of the ground-states of the Coulomb interaction Hamiltonian. Because of the single particle topology of MATBG, the two flat bands at each valley and spin bands can be labeled by a Chern number $C = 1$ and $C = -1$, related by C_2T symmetry [19,28,29,48–51]. In the chiral flat limit, at each filling ν, the interaction favors the successive occupation of such Chern bands, leading to many-body degenerate ground states at filling ν with Chern number $(4\text{-}|\nu|), (2\text{-}|\nu|), \ldots, (|\nu| - 2), (|\nu| - 4)$. We interpret these "chiral-flat" limit states as the low-energy states which compete against each other.

Perturbation away from the chiral limit predicts that the states with the lowest Chern numbers win. Hence at filling $\nu = 0, \pm 2$ the theoretical ground states have $C = 0$, while at $\nu = \pm 1, \pm 3$ they have $|C| = 1$, all of which are now ferromagnetic in a lower $\mathrm{U}(4)$ symmetry. A B field lowers the energy of the large Chern numbers and at filling $\nu = \pm 1$ a first order phase transition between the low-field $|C| = 1$ ground state and the high-field $|C| = 3$ ground state is predicted to occur at $B_2 = 0.5$ T [30]. At filling $\nu = \pm 2$ a first order phase transition between the low-field $|C| = 0$ ground state and the high-field $|C| = 2$ ground state is predicted to occur at $B_1 = 0.2$ T. Perturbation theory also predicts the polarization of the CCIs upon introduction of kinetic energy, when the symmetry of the system lowers even further to $\mathrm{U}(2)$ spin-charge rotation per valley. The Chern number $C = 0$ and $0 < |C| < 4 - |\nu|$ states at integer fillings ν are fully and partially intervalley coherent [Figs. 4(f) and 4(g)], while the states with Chern number $|C| = 4 - |\nu|$ are valley polarized. Numerical results based on exact diagonalization and DMRG [19,48,52] suggest that some of the CCI ground states, particularly at $\nu = \pm 3$, do not survive for realistic parameters, and that a competition occurs between (nematic) metal, momentum $M(\pi)$

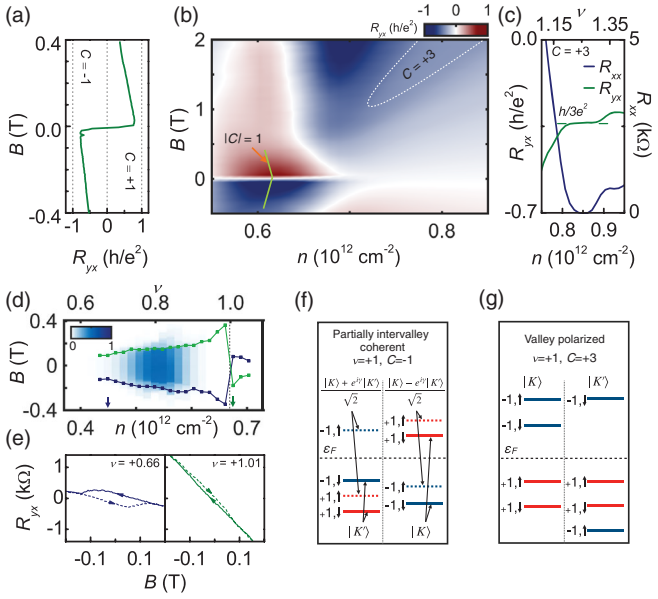

FIG. 4. (a) R_{yx} vs B taken along the green line in (b). (b) R_{yx} vs n and B close to $\nu = +1$. A CCI zero-field CCI with $C = -1$ and a high-field CCI with $C = 3$ (white line). (c) R_{yx} and R_{xx} vs n taken at $B = 2.5$ T shows fully quantized $h/3e^2$ plateau. (d) AHE resistance $\Delta R_{yx}/2$ vs n and B where green and blue symbols show coercive field values. (e) R_{yx} vs B line traces taken at corresponding n in (d). (f),(g) Schematics of the $C = -1$ and $C = +3$ states at filling $\nu = +1$. For $C = -1$, we propose a partially intervalley coherent state, while for $C = +3$ a valley polarized state.

stripe, and K-CDW orders and metallic states with no broken symmetries.

Comparing to experiment, at $\nu = \pm 2$ we find agreement with theory with a zero field Chern number $C = 0$ state and an in-field $|C| = 2$ state. In zero field at $\nu = +3$, the experiment finds $C = 0$, while for $\nu = -3$ we find neither a CI nor a CCI. These zero-field states conflict with the perturbation-derived $|C| = 1$ states, however at high B field these transition to $|C| = 1$ states, as predicted by theory. We find that the theoretically predicted low field $|C| = 1$ state is the only possible option arising from a translationally invariant interaction driven Chern bands at $\nu = \pm 3$, although $C = 0$ insulators are allowed if mixing with remote bands plays a role [31]. Its absence could suggest the presence of translational symmetry-broken states at this filling, which is further supported by numerical results [30]. At $\nu = +1$, the experimental discovery, presented here of a $|C| = 1$ is in tune with the theoretically predicted ground state. Most strikingly, the in-field transition from the $|C| = 1$ to the higher, $|C| = 3$ state also corresponds to the theoretically predicted state.

We examine the B-field induced transitions at $\nu = +1$ filling in Fig. 4(b), which shows R_{yx} vs n and B. For $B < 0.5$ T the phase diagram is mainly defined by the AHE hysteresis loop on the hole doped side of $\nu < +1$. The center of the hysteresis loop shifts in B field in agreement with the Streda formula for a Chern number of $C = -1$ for positive and $C = +1$ for negative B field [Fig. 4(a)]. The sign of the Chern numbers is consistent with the sign of R_{yx} for the AHE, which maintains positive values in positive B, while the normal Hall effect at higher n produces a negative R_{yx}. While ΔR_{yx} is strongest around $\nu \approx +0.84$, close to $\nu = +1$ it is strongly suppressed and its coercive B-field values are increased [Fig. 4(d) and Supplemental Matieral Figs. 4 and 5]. Sharply at $\nu > +1$ we observe a sign reversal of ΔR_{yx}. Changes in the sign and magnitude of the hysteresis loop across the gap are expected of CCI and indicates a sign change of the Chern number across the $\nu = +1$ gap [45,53] [see Supplemental Material [43] and Fig. 4(e)]. The low field CCI states gradually disappear above $B > 0.5$ T, and we observe the onset of an CCI which also follows the Streda formula with Chern number of $C = +3$ and shows well quantized Hall plateaus $R_{yx} = h/3e^2$ ($R_{xx} = 0\ \Omega$) shown in Fig. 4(c).

To summarize—our findings shed new light on the underlying ground states of MATBG, and show that even in zero field these form nearly degenerate and competing interaction-induced Chern insulators, which can be further tuned by weak magnetic and electric fields. While a general picture emerges, the hierarchy of the degenerate ground states still needs to be understood. Here, while for the $\nu = +1$ state theory predicts $C = \pm 1$ for zero field, and $C = \pm 3$ for elevated field, in the experiment we observe only $C = -1$ and $C = +3$, respectively. The physical origin of this symmetry breaking could lie in sample imperfections, which are not covered by our theoretical model, like domain walls [54], strain variations [55] or h-BN alignment [56], though it also may lie in the many-body interactions, which at this point however are notoriously challenging to model in nonzero fields. To fully understand the phase diagram of MATBG in all its details further experimental and theoretical work will be needed.

We are grateful for fruitful discussions with Frank H. L. Koppens and Ashvin Vishwanath. D. K. E. acknowledges support from the Ministry of Economy and Competitiveness of Spain through the "Severo Ochoa" program for Centres of Excellence in R&D (SE5-0522), Fundació Privada Cellex, Fundació Privada Mir-Puig, the Generalitat de Catalunya through the CERCA program, funding from the European Research Council (ERC) under the European Union's Horizon 2020 research and innovation programme (Grant No. 852927) and the La Caixa Foundation. B. A. B. was supported by the DOE Grant No. DE-SC0016239, the Schmidt Fund for Innovative Research, Simons Investigator Grant No. 404513, the Packard Foundation, the Gordon and Betty Moore Foundation through Grant No. GBMF8685 toward the Princeton theory program, and a Guggenheim Fellowship from the John Simon Guggenheim Memorial Foundation.

Further support was provided by the NSF-EAGER No. DMR 1643312, NSF-MRSEC No. DMR-1420541 and DMR-2011750, ONR No. N00014-20-1-2303, Gordon and Betty Moore Foundation through Grant No. GBMF8685 toward the Princeton theory program, BSF Israel U.S. foundation No. 2018226, and the Princeton Global Network Funds. A. H. M. and M. X. were supported by DOE Grant No. DE-FG02-02ER45958 and Welch Foundation Grant No. F1473. P. S. acknowledges support from the European Union's Horizon 2020 research and innovation programme under the Marie Skłodowska-Curie Grant No. 754510.

D. K. E. and P. S. conceived and designed the experiments; P. S. fabricated the devices and performed the measurements; P. S., D. K. E., B. A. B., M. X., and A. H. M. analyzed the data; B. A. B., M. X., and A. H. M. performed the theoretical modeling; T. T. and K. W. contributed materials; D. K. E. and X. L. supported the experiments: P. S., D. K. E., B. A. B, M. X., and A. H. M. wrote the paper.

The authors claim no competing interest.

*Corresponding author.
petr.stepanov@icfo.eu
†Corresponding author.
dmitri.efetov@icfo.eu

[1] Y. Cao, V. Fatemi, A. Demir, S. Fang, S. L. Tomarken, J. Y. Luo, J. D. Sanchez-Yamagishi, K. Watanabe, T. Taniguchi, E. Kaxiras, R. C. Ashoori, and P. Jarillo-Herrero, Correlated insulator behaviour at half-filling in magic-angle graphene superlattices, Nature (London) **556**, 80 (2018).

[2] X. Lu, P. Stepanov, W. Yang, M. Xie, M. A. Aamir, I. Das, C. Urgell, K. Watanabe, T. Taniguchi, G. Zhang, A. Bachtold, A. H. MacDonald, and D. K. Efetov, Superconductors, orbital magnets, and correlated states in magic angle bilayer graphene, Nature (London) **574**, 653 (2019).

[3] D. Wong, K. P. Nuckolls, M. Oh, B. Lian, Y. Xie, S. Jeon, K. Watanabe, T. Taniguchi, B. A. Bernevig, and A. Yazdani, Cascade of electronic transitions in magic-angle twisted bilayer graphene, Nature (London) **582**, 198 (2020).

[4] U. Zondiner, A. Rozen, D. Rodan-Legrain, Y. Cao, R. Queiroz, T. Taniguchi, K. Watanabe, Y. Oreg, F. von Oppen, A. Stern, E. Berg, P. Jarillo-Herrero, and S. Ilani, Cascade of phase transitions and Dirac revivals in magic-angle graphene, Nature (London) **582**, 203 (2020).

[5] H. C. Po, L. Zou, A. Vishwanath, and T. Senthil, Origin of Mott Insulating Behavior and Superconductivity in Twisted Bilayer Graphene, Phys. Rev. X **8**, 031089 (2018).

[6] Y. Cao, V. Fatemi, S. Fang, K. Watanabe, T. Taniguchi, E. Kaxiras, and P. Jarillo-Herrero, Unconventional superconductivity in magic-angle graphene superlattices, Nature (London) **556**, 43 (2018).

[7] J. F. Dodaro, S. A. Kivelson, Y. Schattner, X. Q. Sun, and C. Wang, Phases of a phenomenological model of twisted bilayer graphene, Phys. Rev. B **98**, 075154 (2018).

[8] F. Xie, Z. Song, B. Lian, and B. A. Bernevig, Topology-Bounded Superfluid Weight in Twisted Bilayer Graphene, Phys. Rev. Lett. **124**, 167002 (2020).

[9] M. Yankowitz, S. Chen, H. Polshyn, Y. Zhang, K. Watanabe, T. Taniguchi, D. Graf, A. F. Young, and C. R. Dean, Tuning superconductivity in twisted bilayer graphene, Science **363**, 1059 (2019).

[10] P. Stepanov, I. Das, X. Lu, A. Fahimniya, K. Watanabe, T. Taniguchi, F. H. L. Koppens, J. Lischner, L. Levitov, and D. K. Efetov, Untying the insulating and superconducting orders in magic-angle graphene, Nature (London) **583**, 375 (2020).

[11] L. Balents, C. R. Dean, D. K. Efetov, and A. F. Young, Superconductivity and strong correlations in Moiré flat bands, Nat. Phys. **16**, 725 (2020).

[12] F. Wu, A. H. Macdonald, and I. Martin, Theory of Phonon-Mediated Superconductivity in Twisted Bilayer Graphene, Phys. Rev. Lett. **121**, 257001 (2018).

[13] B. Lian, Z. Wang, and B. A. Bernevig, Twisted Bilayer Graphene: A Phonon-Driven Superconductor, Phys. Rev. Lett. **122**, 257002 (2019).

[14] J. González and T. Stauber, Kohn-Luttinger Superconductivity in Twisted Bilayer Graphene, Phys. Rev. Lett. **122**, 026801 (2019).

[15] H. Isobe, N. F. Q. Yuan, and L. Fu, Unconventional Superconductivity and Density Waves in Twisted Bilayer Graphene, Phys. Rev. X **8**, 041041 (2018).

[16] C.-C. Liu, L.-D. Zhang, W.-Q. Chen, and F. Yang, Chiral Spin Density Wave and $d + id$ Superconductivity in the Magic-Angle-Twisted Bilayer Graphene, Phys. Rev. Lett. **121**, 217001 (2018).

[17] R. Bistritzer and A. H. MacDonald, Moire bands in twisted double-layer graphene, Proc. Natl. Acad. Sci. U.S.A. **108**, 12233 (2011).

[18] M. Koshino, N. F. Q. Yuan, T. Koretsune, M. Ochi, K. Kuroki, and L. Fu, Maximally Localized Wannier Orbitals and the Extended Hubbard Model for Twisted Bilayer Graphene, Phys. Rev. X **8**, 031087 (2018).

[19] J. Kang and O. Vafek, Strong Coupling Phases of Partially Filled Twisted Bilayer Graphene Narrow Bands, Phys. Rev. Lett. **122**, 246401 (2019).

[20] I. Das, X. Lu, J. Herzog-Arbeitman, Z.-D. Song, K. Watanabe, T. Taniguchi, B. A. Bernevig, and D. K. Efetov, Symmetry-broken Chern insulators and Rashba-like Landau-level crossings in magic-angle bilayer graphene, Nat. Phys. **17**, 710 (2021).

[21] K. P. Nuckolls, M. Oh, D. Wong, B. Lian, K. Watanabe, T. Taniguchi, B. A. Bernevig, and A. Yazdani, Strongly correlated Chern insulators in magic-angle twisted bilayer graphene, Nature (London) **588**, 610 (2020).

[22] S. Wu, Z. Zhang, K. Watanabe, T. Taniguchi, and E. Y. Andrei, Chern insulators, van Hove singularities and topological flat bands in magic-angle twisted bilayer graphene, Nat. Mater. **20**, 488 (2021).

[23] Y. Saito, J. Ge, L. Rademaker, K. Watanabe, T. Taniguchi, D. A. Abanin, and A. F. Young, Hofstadter subband ferromagnetism and symmetry-broken Chern insulators in twisted bilayer graphene, Nat. Phys. **17**, 478 (2021).

[24] Y. Saito, F. Yang, J. Ge, X. Liu, T. Taniguchi, K. Watanabe, J. I. A. Li, E. Berg, and A. F. Young, Isospin Pomeranchuk

effect in twisted bilayer graphene, Nature (London) **592**, 220 (2021).
[25] Y. Choi, H. Kim, Y. Peng, A. Thomson, C. Lewandowski, R. Polski, Y. Zhang, H. S. Arora, K. Watanabe, T. Taniguchi, J. Alicea, and S. Nadj-Perge, Correlation-driven topological phases in magic-angle twisted bilayer graphene, Nature (London) **589**, 536 (2021).
[26] R. Bistritzer and A. H. Macdonald, Moiré bands in twisted double-layer graphene, Proc. Natl. Acad. Sci. U.S.A. **108**, 12233 (2011).
[27] M. Koshino, N. F. Q. Yuan, T. Koretsune, M. Ochi, K. Kuroki, and L. Fu, Maximally Localized Wannier Orbitals and the Extended Hubbard Model for Twisted Bilayer Graphene, Phys. Rev. X **8**, 031087 (2018).
[28] J. Kang and O. Vafek, Symmetry, Maximally Localized Wannier States, and a Low-Energy Model for Twisted Bilayer Graphene Narrow Bands, Phys. Rev. X **8**, 031088 (2018).
[29] M. Xie and A. H. MacDonald, Nature of the Correlated Insulator States in Twisted Bilayer Graphene, Phys. Rev. Lett. **124**, 097601 (2020).
[30] B. Lian, Z.-D. Song, N. Regnault, D. K. Efetov, A. Yazdani, and B. A. Bernevig, TBG IV: Exact insulator ground states and phase diagram of twisted bilayer graphene, arXiv:2009.13530.
[31] M. Xie and A. H. MacDonald, Weak-field Hall resistivity and spin/valley flavor symmetry breaking in MATBG, arXiv:2010.07928.
[32] Y. Saito, J. Ge, K. Watanabe, T. Taniguchi, and A. F. Young, Independent superconductors and correlated insulators in twisted bilayer graphene, Nat. Phys. **16**, 926 (2020).
[33] H. S. Arora, R. Polski, Y. Zhang, A. Thomson, Y. Choi, H. Kim, Z. Lin, I. Z. Wilson, X. Xu, J.-H. Chu, K. Watanabe, T. Taniguchi, J. Alicea, and S. Nadj-Perge, Superconductivity in metallic twisted bilayer graphene stabilized by WSe_2, Nature (London) **583**, 379 (2020).
[34] X. Liu, Z. Wang, K. Watanabe, T. Taniguchi, O. Vafek, and J. I. A. Li, Tuning electron correlation in magic-angle twisted bilayer graphene using Coulomb screening, Science **371**, 1261 (2021).
[35] F. K. de Vries, E. Portoles, G. Zheng, T. Taniguchi, K. Watanabe, T. Ihn, K. Ensslin, and P. Rickhaus, Gate-defined Josephson junctions in magic-angle twisted bilayer graphene, arXiv:2011.00011.
[36] D. Rodan-Legrain, Y. Cao, J. M. Park, S. C. de la Barrera, M. T. Randeria, K. Watanabe, T. Taniguchi, and P. Jarillo-Herrero, Highly tunable junctions and nonlocal Josephson effect in magic angle graphene tunneling devices, arXiv:2011.02500.
[37] B. Lian, X.-Q. Sun, A. Vaezi, X.-L. Qi, and S.-C. Zhang, Topological quantum computation based on chiral Majorana fermions, Proc. Natl. Acad. Sci. U.S.A. **115**, 10938 (2018).
[38] K. Nomura and A. H. MacDonald, Quantum Hall Ferromagnetism in Graphene, Phys. Rev. Lett. **96**, 256602 (2006).
[39] Y. J. Song, A. F. Otte, Y. Kuk, Y. Hu, D. B. Torrance, P. N. First, W. A. de Heer, H. Min, S. Adam, M. D. Stiles, A. H. MacDonald, and J. A. Stroscio, High-resolution tunnelling spectroscopy of a graphene quartet, Nature (London) **467**, 185 (2010).
[40] A. F. Young, C. R. Dean, L. Wang, H. Ren, P. Cadden-Zimansky, K. Watanabe, T. Taniguchi, J. Hone, K. L. Shepard, and P. Kim, Spin and valley quantum Hall ferromagnetism in graphene, Nat. Phys. **8**, 550 (2012).
[41] M. Serlin, C. L. Tschirhart, H. Polshyn, Y. Zhang, J. Zhu, K. Watanabe, T. Taniguchi, L. Balents, and A. F. Young, Intrinsic quantized anomalous Hall effect in a Moiré heterostructure, Science **367**, 900 (2020).
[42] A. L. Sharpe, E. J. Fox, A. W. Barnard, J. Finney, K. Watanabe, T. Taniguchi, M. A. Kastner, and D. Goldhaber-Gordon, Emergent ferromagnetism near three-quarters filling in twisted bilayer graphene, Science **365**, 605 (2019).
[43] See Supplemental Material at http://link.aps.org/supplemental/10.1103/PhysRevLett.127.197701 for full characterization of the SC states.
[44] G. Chen, A. L. Sharpe, E. J. Fox, Y.-H. Zhang, S. Wang, L. Jiang, B. Lyu, H. Li, K. Watanabe, T. Taniguchi, Z. Shi, T. Senthil, D. Goldhaber-Gordon, Y. Zhang, and F. Wang, Tunable correlated Chern insulator and ferromagnetism in a Moiré superlattice, Nature (London) **579**, 56 (2020).
[45] H. Polshyn, J. Zhu, M. A. Kumar, Y. Zhang, F. Yang, C. L. Tschirhart, M. Serlin, K. Watanabe, T. Taniguchi, A. H. MacDonald, and A. F. Young, Electrical switching of magnetic order in an orbital Chern insulator, Nature (London) **588**, 66 (2020).
[46] S. Chen, M. He, Y.-H. Zhang, V. Hsieh, Z. Fei, K. Watanabe, T. Taniguchi, D. H. Cobden, X. Xu, C. R. Dean, and M. Yankowitz, Electrically tunable correlated and topological states in twisted monolayer-bilayer graphene, Nat. Phys. **17**, 374 (2021).
[47] P. Streda, Theory of quantised Hall conductivity in two dimensions, J. Phys. C **15**, L717 (1982).
[48] N. Bultinck, E. Khalaf, S. Liu, S. Chatterjee, A. Vishwanath, and M. P. Zaletel, Ground State and Hidden Symmetry of Magic-Angle Graphene at Even Integer Filling, Phys. Rev. X **10**, 0031034 (2020).
[49] Z. Song, Z. Wang, W. Shi, G. Li, C. Fang, and B. A. Bernevig, All Magic Angles in Twisted Bilayer Graphene Are Topological, Phys. Rev. Lett. **123**, 0036401 (2019).
[50] H. C. Po, L. Zou, T. Senthil, and A. Vishwanath, Faithful tight-binding models and fragile topology of magic-angle bilayer graphene, Phys. Rev. B **99**, 195455 (2019).
[51] J. Liu and X. Dai, Theories for the correlated insulating states and quantum anomalous Hall phenomena in twisted bilayer graphene, Phys. Rev. B **103**, 035427 (2021).
[52] F. Xie, A. Cowsik, Z. Son, B. Lian, B. A. Bernevig, and N. Regnault, TBG VI: An exact diagonalization study of twisted bilayer graphene at nonzero integer fillings, arXiv:2010.00588.
[53] J. Zhu, J.-J. Su, and A. H. MacDonald, Voltage-Controlled Magnetic Reversal in Orbital Chern Insulators, Phys. Rev. Lett. **125**, 227702 (2020).
[54] A. T. Pierce, Y. Xie, J. M. Park, E. Khalaf, S. H. Lee, Y. Cao, D. E. Parker, P. R. Forrester, S. Chen, K. Watanabe, T. Taniguchi, A. Vishwanath, P. Jarillo-Herrero, and A. Yacoby, Unconventional sequence of correlated Chern insulators in magic-angle twisted bilayer graphene, Nat. Phys. (2021), https://doi.org/10.1038/s41567-021-01347-4.

[55] D. E. Parker, T. Soejima, J. Hauschild, M. P. Zaletel, and N. Bultinck, Strain-Induced Quantum Phase Transitions in Magic-Angle Graphene, Phys. Rev. Lett. **127**, 027601 (2021).

[56] J. Shi, J. Zhu, and A. H. MacDonald, Moiré commensurability and the quantum anomalous Hall effect in twisted bilayer graphene on hexagonal boron nitride, Phys. Rev. B **103**, 075122 (2021).